**Article:**
Birnie, C, Chambers, K, Angus, D orcid.org/0000-0003-0734-7835 et al. (1 more author) (2016) Analysis and models of pre-injection surface seismic array noise recorded at the Aquistore carbon storage site. Geophysical Journal International, 206 (2). pp. 1246-1260. ISSN 0956-540X

https://doi.org/10.1093/gji/ggw203

# Analysis and models of pre-injection surface seismic array noise recorded at the Aquistore carbon storage site

Claire Birnie, Kit Chambers, Doug Angus, Anna Stork

Resubmission - May 2016

## Abstract

Noise is a persistent feature in seismic data and so poses challenges in extracting increased accuracy in seismic images and physical interpretation of the subsurface. In this paper, we analyse passive seismic data from the Aquistore carbon capture and storage pilot project permanent seismic array to characterise, classify and model seismic noise. We perform noise analysis for a three month subset of passive seismic data from the array and provide conclusive evidence that the noise field is not white, stationary, or Gaussian; characteristics commonly yet erroneously assumed in most conventional noise models. We introduce a novel noise modelling method that provides a significantly more accurate characterisation of real seismic noise compared to conventional methods, which is quantified using the Mann-Whitney-White statistical test. This method is based on a statistical covariance modelling approach created through the modelling of individual noise signals. The identification of individual noise signals, broadly classified as stationary, pseudo-stationary and non-stationary, provides a basis on which to build an appropriate spatial and temporal noise field model. Furthermore, we have developed a workflow to incorporate realistic noise models within synthetic seismic datasets providing an opportunity to test and analyse detection and imaging algorithms under realistic noise conditions.

## 1 Introduction

Noise is an inevitable feature of seismic data, given that the earth is dynamic, instruments are not perfect and our understanding of physics is still not complete such that even signals originating from the desired

source can prove problematic for seismic processing (i.e. mulitples or ground roll) [e.g., Li et al., 1994; Kahrizi et al., 2014]. For passive seismic data, noise is even more problematic due to the inherent uncertainty in the temporal and spatial location of seismic events. Furthermore, the masking of relatively weak microseismic events by noise leads to one of the main issues in passive seismic monitoring which is increased uncertainty in identifying event arrivals [Bardainne et al., 2009; Maxwell, 2014]. The presence of coherent noise in seismic imaging can result in the introduction of artefacts, while in seismic inversion it can lead to errors in the estimated velocity model and predicted source parameters [Forghani-Arani, 2013]. Synthetic seismic datasets provide a confidence limit under which passive seismic processing and imaging algorithms can be used to accurately identify an event [e.g., Price et al., 2015] and its failure mechanism [e.g., Trifu et al., 2000], such as fracture location, orientation and length. To provide more realistic synthetic seismic data, noise with Gaussian characteristics is commonly added. Over the past few decades, the Gaussian noise assumption has resulted in many techniques being developed specifically to suppress Gaussian noise [e.g., Green et al., 1966; Berkner and Wells Jr, 1998; Bekara et al., 2003]. However, the choice of Gaussian noise is mainly to simplify implementation or demonstrate mathematical properties such as optimality and unbiasedness, rather than based upon physical principles. In many ways, Gaussian noise only serves to obscure seismic arrivals or events rather than providing a sufficiently robust test of processing and imaging algorithms.

What is noise? For passive seismic monitoring scenarios, every recorded signal other than the first arrival P and S waves is typically considered noise, such as ambient noise as well as seismic multiples and mode conversions. Ambient noise, sometimes referred to as background noise, originates from a wide range of sources that can be separated into natural processes and urban activities, dependent on their frequency content [Gutenberg, 1958; Asten, 1978]. Noise below 1 Hz consists of microseisms created by large-scale meteorological events and oceanic waves along the coast [Asten and Henstridge, 1984]. Between 1 and 5 Hz noise sources are likely to be local meteorological events or urban activity and sources above 5 Hz sources are likely to be urban in origin [Bonnefoy-Claudet et al., 2006]. Studies of meteorological noise suggest that wind and rain can have a distinct effect on the noise signature of seismic data [e.g., Nørmark, 2011; Barajas-Olalde and Jeffreys, 2014]. In terms of urban noise, Riahi and Gerstoft [2015] characterised the seismic footprint of traffic and were able to distinguish sources such as trains, aircraft and road traffic. In addition to ambient and urban noise in many oil and gas producing environments there is also production-induced noise resulting from fluid extraction and injection processes. For hydraulic fracture monitoring pumping noise is pervalent, where increased noise levels are observed at stations closer to treatment wells [e.g., Drew et al., 2012; Schilke et al., 2014] broadly above the expected induced seismicity. It should be noted, however, that ambient noise interferometry on passive seismic data has been used increasingly to image subsurface velocity distributions

[e.g., Draganov et al., 2004] and recently multiples are being used to improve event location algorithms [e.g., Belayouni et al., 2015].

Noise analyses have also focussed on noise characteristics (rather than their origin) by investigating the stationarity and Gaussianity of the noise field. A stationary time series is defined to have a constant mean and variance while a Gaussian time series must arise from a Gaussian distribution determined by the mean and variance. In this paper, we note that the terms stationarity and 'Gaussianity' refer to a measure by which a time series is stationary or Gaussian, respectively. It is commonly accepted that noise can only be assumed stationary over a short time period [Riahi et al., 2013] due to contamination of stationary background noise by transient phenomena that are non-stationary in both time and space, such as urban seismic noise [Groos and Ritter, 2009]. Advancements in signal processing have led to the use of noise surrogates to test the stationarity of a time series and provided an index on the strength of stationarity that a time-series exhibits [Borgnat et al., 2010]. The use of surrogates has been applied to study background noise in land-seismic prospecting by Zhong et al. [2015] who concluded that background noise is "not strictly stationary" and as the length of time of the sample increases the stationarity decreases.

The assumption that background noise is Gaussian has gone relatively uncontested since White [1984] discussed the difficulty in testing unambiguously whether seismic noise is Gaussian. A recent investigation by Zhong et al. [2015] used a higher-order spectral analysis method to investigate Gaussianity of background noise with respect to time. They concluded that for periods over 20 seconds noise appears to be Gaussian whereas for periods of the order of 1 second noise is non-Gaussian. Pierce [1997] proposed that seismic noise is likely to have heavier tails than a Gaussian distribution and therefore may be more likely to follow an alpha-stable distribution (note that Gaussian distribution is a subset of an alpha-stable distribution with $\alpha = 2$).

Despite the evidence that noise does not conform to the white, Gaussian noise (WGN) assumption (see next section for definitions), the majority of published approaches still use WGN to test the robustness of event imaging and detection algorithms with respect to noise [e.g., Grion et al., 2015; Berkhout and Blacquière, 2015; Shao et al., 2015; Trojanowski and Eisner, 2015]. Pearce and Barley [1977] included the effect of noise on synthetic seismograms by convolving a sample of recorded noise with broadband white noise creating coloured, Gaussian noise as opposed to the simple WGN approach. However, this approach only serves to produce a distorted signal by weighting the sampled recorded noise by a signal having Gaussian distribution and so is not meaningful. A more deterministic noise modelling method is that of distributed surface sources where source properties, such as direction, amplitude and source time functions, are randomly distributed [e.g., Sylvette et al., 2006; Lunedei and Albarello, 2015; Dean et al., 2015]. While this modelling method

provides significant improvements on the WGN modelling assumption, it is a theoretical modelling method independent of recorded noise and therefore has limitations to the extent to which it can model the complex properties of recorded noise. This is discussed by Dean et al. [2015] who state "Although the modeled data have the same characteristics as the field measurements, it is unlikely that models can be built with the geologic, geographic, and meteorological detail required to create accurate models". A recent advancement in representing realistic noise in synthetic datasets is to directly incorporate a sample of recorded noise into the synthetic dataset (referred to as a 'cut-and-paste' job). This technique leads to a so-called semi-synthetic dataset and can be used for robustness tests as shown by Chambers et al. [2010] and Forghani-Arani et al. [2012]. Although the semi-synthetic approach provides sufficient realism, it does not allow one to modify the temporal and spatial statistical characteristics of noise in a methodological manner. Furthermore, it requires having real noise recorded from the array, where in many cases it may be desirable to simulate noise levels prior to acquisition.

Since processing and imaging algorithms tend to be tested under a WGN assumption, it is often unclear how an algorithm will handle noise from a field dataset, leading to uncertainty in the accuracy of identified events and their derived properties. In this paper we investigate statistical methods for analysing and introduce a new modelling approach for seismic noise. We begin with a theoretical description of how noise is characterised before describing three existing techniques for noise simulation. We also propose a new modelling approach (ICOVA) based on the covariance modelling method. We then analyse and compare noise models against observations from three months of passive seismic data collected at the Aquistore carbon storage site. We observe and confirm that noise does not conform to the stationary, white, and Gaussian assumptions typically used by traditional noise modelling methods. We find that whilst the existing approaches fail to adequately simulate the noise characteristics due to their constraining assumptions the new ICOVA modelling approach provides more faithful representations for the noise field. The results of this study have possible implications for the design and implementation of noise cancellation and detection algorithms, the development of more robust noise models as well as improved survey designs. The relevance of more realistic noise modelling is potentially not limited to passive seismic applications and has potential for active source surface reflection and time-lapse seismic applications.

## 2 Theory

The traditional WGN modelling method assumes noise conforms to all of the following statistical properties:

1. **stationary** requiring that the first and second mathematical moments (mean and variance, respec-

tively) are constant over the sample dimension in which stationarity is being determined,

2. exhibits a **white power spectrum** requiring the noise to have a constant power spectral density (PSD), such that energy is distributed equally across all frequencies, and
3. **Gaussian** requiring the noise to have a probability density function equal to that of a single-variate Gaussian distribution and therefore the distribution can be completely described by only the first and second mathematical moments.

The first section discusses the methods used to investigate whether noise conforms to the aforementioned assumptions. The second section details some of the common statistical noise modelling techniques, where we introduce some new techniques to characterise the noise field.

## 2.1 Noise characterisation

If noise is spatially and temporally stationary, the signal should display a constant mean and variance in both space and time coordinates. We compute the mean and variance using a sliding window analysis with a window length of 5 seconds and a window overlap of half the window length. The analysis window is chosen to correspond with those used in surface microseismic applications, which wish to contain a P-wave moveout across the array (1-2 seconds ) and allow an additional buffer either side of the window. The window size and overlap enables capturing of any rapid changes in mean and variance in the data. Although a short window increases the computational expense, a longer window would smooth the results and lose important spatial and temporal resolution at the expense of computational efficiency.

To consider whether the noise power spectrum is white, we compute the PSD over an hour period and a short-time Fourier Transform (STFT) using the same sliding window analysis as done with the mean and variance calculations. The PSD characterises the overall power spectrum over a full hour whereas the STFT characterises any changes in the power spectrum over a much smaller time scale. To consider if the total energy is distributed equally across the array, the seismic energy (i.e. the squared amplitude) is computed using the same sliding window analysis as done with the STFT calculation.

The final noise property analysed is the extent to which the seismic noise is Gaussian. We consider only two methods to determine the distribution shape of seismic noise. Both techniques are based on the third and fourth mathematical moments that describe the skewness and kurtosis (i.e., 'peakedness') of a distribution, respectively. The first technique is performed in the time domain and uses the mathematical moments directly, while the second technique is performed in the frequency domain and uses cumulants.

The first technique is the conventional method of statistical moments. The first and second moments are the

well known mean and variance, respectively, and the third and fourth moments are skewness and kurtosis, respectively. Skewness ($\gamma_1$) and kurtosis ($\gamma_2$) are defined:

$$\gamma_1 = \frac{\mu_3}{\sigma^3} = \frac{E[(x-\mu)^3]}{E[(x-\mu)^2]^{3/2}} \tag{1}$$

and

$$\gamma_2 = \frac{\mu_4}{\sigma^4} = \frac{E[(x-\mu)^4]}{E[(x-\mu)^2]^2}, \tag{2}$$

where $x$ is a data point, $\mu$ is the first mathematical moment (i.e. mean), $\mu_i$ is the $i$th mathematical moment, $\sigma$ is the standard deviation and $E[\cdot]$ denotes the expectation operator. For a Gaussian distribution, both skewness and excess kurtosis are equal to zero, where excess kurtosis is defined as $\gamma_{2_{ex}} = \gamma_2 - 3$. The moments are calculated using the same sliding window analysis as performed on the stationarity test for mean and variance.

An extension to the conventional method of statistical moments is the analysis of cumulants and is performed using Higher Order Spectral Analysis (HOSA) and are commonly used in statistical signal processing [e.g., Bartelt et al., 1984; Walden and Williams, 1993; Pflug, 2000]. The HOSA method applied here considers the bispectrum and trispectrum, which are the Fourier transforms of the third- and fourth-order cumulants, respectively. Cumulants are an alternative to mathematical moments and arise from the natural logarithm of the mathematical moments [Fisher, 1930]. By using cumulants the dependence on lower order moments (i.e., mean and variance) is removed [Collis et al., 1998]. The squared magnitude of the normalised bispectrums and trispectrums results in the bicoherence ($\hat{b}^2$) and tricoherence ($\hat{t}^2$), respectively:

$$\hat{b}^2(f_1, f_2) = \frac{|\frac{1}{N}\sum_{i=1}^{N}[X_i(f_1)X_i(f_2)X_i^*(f_1+f_2)]|^2}{\hat{P}(f_1)\hat{P}(f_2)\hat{P}(f_1+f_2)} \tag{3}$$

and

$$\hat{t}^2(f_1, f_2, f_3) = \frac{|\frac{1}{N}\sum_{i=1}^{N}[X_i(f_1)X_i(f_2)X_i(f_3)X_i^*(f_1+f_2+f_3)]|^2}{\hat{P}(f_1)\hat{P}(f_2)\hat{P}(f_3)\hat{P}(f_1+f_2+f_3)}, \tag{4}$$

where $\hat{P}(f) = < X(f)X^*(f) >$ (<> denotes the expectation estimator), $X$ is the Fourier transform of a time-series $x$, and $X^*$ is the complex conjugate of $X$.

Both equations 3 and 4 are zero for Gaussian distributions and can reach a maximum of one for non-Gaussian

distributions [Chandran et al., 1994]. The coherence calculations require $N$ realisations of the distribution and compute a value for every possible frequency combination of $f_1$ and $f_2$ for bicoherence and $f_1$, $f_2$ and $f_3$ for tricoherence. To get a single value of coherence with respect to space and time the full coherence array for a time window at one position in space is averaged. The coherence analysis is computed on an hour of data using a 2 second realisation window and 30 realisations per calculation (i.e., one coherence value per minute of data). To provide a benchmark for the computed values, a Gaussian surrogate noise is created using the mean and variance of each data sample used to compute the Gaussianity property. (Note that this method of creating surrogates differs from that commonly used in communication theory which is performed in the frequency domain, see for example Borgnat et al. [2010].)

## 2.2 Noise modelling procedures

In this section, we discuss five approaches to statistically model noise. The first two approaches are used already in seismic noise modelling [for example O'Brien, 1974; Pearce and Barley, 1977] while the remaining three approaches are novel applications to seismic noise modelling adapted from communication theory [for example Massart et al., 1988; Scharf, 1991]. Excluding WGN, all acronyms of modelling methods are not common acronyms and are only used by the authors.

**WGN:** The first noise model is a simple White Gaussian Noise (WGN) model. For the WGN model to be comparable to the recorded noise and the other noise models, the amplitude is scaled to fit the expected range of the recorded noise.

**CONV:** The second noise model, referred to as the CONVolution-based modelling method (CONV), is similar to work by Pearce and Barley [1977] and Zhong et al. [2015], where a period of recorded noise ($\boldsymbol{t}$) is convolved ($*$) with a random Gaussian trace ($\boldsymbol{g}$) to create a modelled trace ($\boldsymbol{n}$) with the same frequency content as the original recorded trace:

$$\boldsymbol{n} = \boldsymbol{t} * \boldsymbol{g}, \tag{5}$$

(bold font indicates a vector quantity). Following Pearce and Barley [1977], noise is modelled on a station-by-station basis with the recorded noise separated into 1 minute time segments. Zhong et al. [2015] have used this method to create surrogate noise models as a test for stationarity.

**COVA:** The third modelling method is based on the statistical COVAriance modelling method (COVA) which assumes that noise can be statistically represented as a multivariate Gaussian random field, defined by only a mean and covariance matrix. A synthetic noise patch is created by drawing a random realization from this multivariate Gaussian distribution as illustrated in the work flow in Figure 1. The data is divided into recorded noise patches defined by a spatial group of $N_x$ traces, over a finite time window, $N_t$, with patch dimensions $[N_t \times N_x]$. For computational purposes, this is reshaped to create a patch column vector, $\boldsymbol{d}$, with dimensions $[N_t N_x \times 1]$. To get a good approximation of the mean and covariance matrix, $K$ realisations of the noise are used (i.e. $K$ patches). The patch vectors are horizontally concatenated to create a data matrix, $\boldsymbol{D}$, with dimensions $[N_t N_x \times K]$:

$$\boldsymbol{D} = [\boldsymbol{d}_1 \ \boldsymbol{d}_2 \ \ldots \ \boldsymbol{d}_{K-1} \ \boldsymbol{d}_K]. \tag{6}$$

Prior to computing the covariance matrix, the mean $\boldsymbol{\mu}$ is calculated across the $K$ realisations

$$\boldsymbol{\mu} = \frac{\boldsymbol{D}\mathbf{1}}{K-1}, \tag{7}$$

where $\mathbf{1}$ is a unit column vector of length $K$. The mean is removed from each patch (i.e. $\hat{\boldsymbol{d}} = \boldsymbol{d} - \boldsymbol{\mu}$) and the covariance matrix $\boldsymbol{C}$ is computed using

$$\boldsymbol{C} = \hat{\boldsymbol{D}}\hat{\boldsymbol{D}}^T/K, \tag{8}$$

where $\hat{\boldsymbol{D}} = [\hat{\boldsymbol{d}}_1 \ \hat{\boldsymbol{d}}_2 \ \ldots \ \hat{\boldsymbol{d}}_{K-1} \ \hat{\boldsymbol{d}}_K]$ and $\hat{\boldsymbol{D}}^T$ is the transpose of $\hat{\boldsymbol{D}}$. $\boldsymbol{C}$ is then decomposed into upper and lower triangular matrices through a Cholesky decomposition

$$\boldsymbol{C} = \boldsymbol{C}^{1/2}\boldsymbol{C}^{T/2}. \tag{9}$$

The lower triangular matrix $\boldsymbol{C}^{1/2}$ is the square root of the covariance matrix $\boldsymbol{C}$ which is the equivalent of standard deviation for univariate normal distributions. A random vector $\boldsymbol{b}$ of Gaussian white noise with unit variance and zero mean is generated to form the basis of the noise model. To recreate the spatio-temporal correlation observed on the noise patches, $\boldsymbol{d}$, the Gaussian noise vector is multiplied by the lower triangular matrix, $\boldsymbol{C}^{1/2}$, and the product is summed with the mean vector, $\boldsymbol{\mu}$,

$$\tilde{\boldsymbol{d}} = \boldsymbol{C}^{1/2}\boldsymbol{b} + \boldsymbol{\mu}. \tag{10}$$

The modelled patch vector $\tilde{\boldsymbol{d}}$ is then reshaped back to the original patch dimensions to produce a modelled noise patch $\tilde{\boldsymbol{D}}$ with the same first and second mathematical moments as a recorded patch $\boldsymbol{d}$. Where the noise field is considered as a single statistical phenomenon, as opposed to the sum of multiple noise signals, the COVA approach uses time segments of the full-array data to make up the noise realisations.

**ICOVA:** Alternatively, the noise can be considered as the sum of multiple phenomena that can have their signals isolated and modelled with spatial and temporal patch lengths varying to represent their statistical properties. For each phenomenon (or noise type) we isolate the relevant data and perform a COVA simulation. The final model is generated by summing the results from the different noise types with the final model being referred to as the isolated COVA (ICOVA) model. The ICOVA method requires multiple realisations of each type of noise signal, having the same statistical properties observed across the realisations. To ensure this condition is met a minimum of 200 realisations were used for each identified noise signal model and all realisations were required to have a $> 75\%$ probability of arising from the same distribution. The probability of arising from the same distribution was determined using a Mann-Whitney-White (MWW) test [Bloomfield, 2014].

**ICOVA-LPF:** The final noise modelling method provides an alternative for modelling individual noise signals where they do not arise from a multivariate Gaussian distribution. This method models a single realisation through the use a Linear Prediction Filter (LPF), where the filter coefficients are determined using the autocorrelation method of autoregressive modelling. The LPF method is used on noise signals that were not accurately represented in the ICOVA model and therefore is the sum of noise signals modelled using ICOVA and LPF methods, and is referred to as the ICOVA-LPF model.

# 3 Surface Array Passive Seismic Data

The seismic data analysed in this study comes from the Aquistore carbon dioxide ($CO_2$) storage site, located in South Saskatchewan, Canada in the northern part of the Williston Basin [Roach et al., 2015]. $CO_2$ is captured at the Boundary Dam power plant to the east of the Aquistore storage site, where some of the $CO_2$ is transported by pipeline to the site. The $CO_2$ is injected into a deep saline aquifer at a depth of 3150-3350m to study geological storage of $CO_2$. Injection started in late April 2015 and the project has injected up to 1000 tonnes per day over an initial injection period of six months.

The permanent passive seismic array consists of 51 buried, vertical component geophones having a cross-

shaped geometry as illustrated in Figure 2 and has been recording since 25 July 2012. The geophones are 10Hz instruments with a sampling frequency of 500Hz buried at a depth of 20m. A North-South (N-S) road passes close to station 1 and an East-West (E-W) road passes close to station 14. A vertical injection and a vertical observation well are located near the centre of the geophone array as illustrated by triangles in Figure 2. Drilling and construction of the injection well occurred between July and September 2012, and drilling and construction of the observation well occurred between September and December 2012. In this study we analyse a subset of the data from 25 July to 5 October 2012. An example of the recorded data is given in Figure 3. Where results are given for a week of data these are computed from 14 August whilst for results computed for an hour these are computed from the Tuesday between 1p.m. and 2p.m.. These time samples are chosen as they are representative of the full dataset. Since the array has been recording prior to $CO_2$ injection, the recorded time series represents an excellent dataset on which to study non-injection related noise signals. During injection periods, addition noise signals would be present in the data, however, the techniques proposed in this study could easily be extended to include this type of noise. To preserve the noise signals of interest, no preprocessing was performed on the data.

# 4 Noise Characterisation

## 4.1 Noise analysis

The stationarity results for a single week are illustrated in Figure 4. There is a clear trend of larger magnitude mean and variance values around the centre of the array with an observable decrease in mean and variance away from the array centre. Similar large magnitude mean and variance values are observed at station 1, where the large mean values are observed for shorter periods of time and are not observed during the night-time. It is likely that the increased values observed at the centre of the array are associated with noise originating from the well site and the increased values at station 1 are likely due to noise arising from road traffic.

PSDs and STFTs for three stations across the EW geophone profile are shown in Figure 5. Comparison of the three PSDs shows that the power spectrum varies significantly across the array, with station 42 in particular experiencing higher energy content at higher frequencies than stations 1 and 51. Station 51 has a constant power spectra across the hour (as shown in the STFT plots), station 1 experiences several spikes across all frequencies, and station 42 experiences a break in the power spectral trend for about a minute at approximately 46 minutes. Figure 6 illustrates the distribution of energy across the array, where higher

energy levels are observed around the well site. Therefore, not only are the individual power spectrums non-white, but the energy across the array is also not equally distributed.

Figure 7 illustrates the distribution of raw amplitudes for three 5-seconds windows with varying levels of Gaussianity. Each plot has a Gaussian probability density function overlain on it that has been computed from the mean and variance of the amplitudes observed in the respective windows. Due to the finite sample length of each window, numerically computed skewness and excess kurtosis values for the Gaussian surrogate noise are non-zero (see Table 1). However, comparison of the Gaussian surrogate with the recorded Aquistore values shows that the recorded noise variations are significantly higher. Table 1 illustrates that the average skewness for the recorded noise is close to zero. Yet, the maximum and minimum values are substantially higher than that of the Gaussian noise. For the excess kurtosis values of the recorded noise the mean is noticeably less than zero and over 70% of the values are less than zero. For the Gaussian surrogates there are no values for either skewness or kurtosis that have a magnitude greater than 1. For the recorded noise 4% of excess kurtosis values have a magnitude greater than one, demonstrating that values of kurtosis have a higher variability in the recorded noise than the Gaussian surrogates. Despite the higher variations in both skewness and excess kurtosis values for the recorded noise, the spatial and temporal trends are much less clear than those observed for the mean and variance in the stationarity analysis, as shown in Figure 8.

Figure 8 shows the bicoherence and tricoherence values for the recorded noise and the Gaussian surrogate noise (Figure 8e,f and 8g, h respectively). While the background trends for the bicoherence and tricoherence analyses are reasonably similar in magnitude to the Gaussian surrogate noise values, there is an observable spatio-temporal structure to the values. The areas of strongest non-Gaussianity are at stations 1 and 2 for times between 13 and 16 minutes, at 35 minutes and between 56 and 58 minutes. At these points both the bicoherence and tricoherence values of the recorded noise are double that of the Gaussian surrogate noise. Other areas of significant non-Gaussianity occur for stations around the well site (i.e. stations 23 to 45), which have on average 20% higher bicoherence and tricoherence magnitudes than the reference Gaussian values. Station 41 appears to display the least Gaussianity with respect to both bicoherence and tricoherence. As well, there are 2 minutes of increased non-Gaussianity between 46 to 47 minutes across stations 23 to 45. As with the method of statistical moments, the variations of kurtosis are greater than skewness.

## 4.2 Noise classification

Next we consider what noise sources may be present in the data and identify three separate noise signals, as illustrated in Figure 9. The first signal (Figure 9a,d) is a constant 60 Hz signal recorded at station 51

to the far east of the array and is believed to be due to electrical interference between power cables and the recording instruments. The second identified signal (Figure 9b,e) is observed on stations adjacent to the roadside (stations 1 and 14), where the signal is characterised by a burst of energy that lasts about one minute with peak energy around the middle of the signal duration. The signal consistently appears as a broad-band burst and the wavelet shape in time is highly variable. In some instances the noise can be observed on neighbouring stations. The final identified noise signal (Figure 9c,f) is characterised by a strong frequency banding with intermittent pauses. The signal is centred around the well site, yet is observable on stations up to 500 metres away with associated attenuation of higher frequency bands.

The presence of at least three broadly different noise signals across the array leads us to postulate that instead of considering the noise field as a single statistical phenomenon, it is more realistic to consider it as the sum of multiple phenomena, each with their own spatial, temporal, frequency and statistical distribution properties as illustrated in the following equation:

$$n(x,t) = a(x,t) + b(x,t) + c(x,t) + \ldots, \tag{11}$$

where $x$ is the spatial coordinate, $t$ is time, $n$ is the full noise field, and $a$, $b$, $c$, ... are individual noise sources. Similar to the work of Priestley [1988], we propose that, for modelling purposes, noise is split into the following three classifications dependent on their temporal properties with respect to a specified event detection window (EDW):

1. *Stationary noise*: a constant signal over the EDW, such as that observed at station 51,
2. *Non-stationary noise*: a signal that does not last for a significant period with respect to the EDW, such as that observed at station 1, and
3. *Pseudo-non-stationary noise*: a constant signal for a significant period with respect to the EDW, yet is not constant over the full EDW, such as that observed at station 41.

In this study the EDW is one hour.

# 5 Noise Modelling Results

Shown in Figure 10 are the noise modelling results and the recorded noise on which they were based. For the CONV modelling, the hour of recorded noise is split into one minute time windows and modelled. These models are then concatenated to represent the temporal location of the recorded noise window from which they have been computed. The COVA method uses a spatial patch length ($N_x$) of 50, a temporal patch

length ($N_t$) of one second and 3600 realisations ($K$) while these parameters vary across individual models in the ICOVA modelling method. For COVA and ICOVA modelling the modelled time lengths are shorter than the recorded noise, therefore a Monte-Carlo simulation is performed to create multiple models from Gaussian basis vectors that are concatenated to create the full time window. Figure 11 displays the modelled noise signals (identified in Figure 9) for the first three noise models (WGN, CONV and COVA) in the time domain and is based on considering the noise field as a whole. Figure 12 is the frequency domain representation of the modelled noise signals shown in Figure 11.

Due to the WGN model being independent of the recorded noise, it is not surprising that this model has little visual similarity with the recorded data. The CONV model shows a good visual correlation in the time domain (Figure 10(c)). However, when analysing the power spectrum for the individual noise signals (i.e., in Figure 9), it is clear that the CONV model fails to characterise the traffic noise (Figure 11(e) and 12(e)). This is expected as this method requires noise to be stationary over the modelling time window and this is not the case for traffic noise. The COVA model also fails to accurately represent traffic noise (Figure 11(h) and 12(h)) due to the modelling requirement that patches must have the same statistical properties. The presence of traffic noise in a handful of patches has resulted in the inclusion of traffic noise in the covariance matrix and therefore also into every modelled noise patch. This is also the case for well-site noise, where the pause at around 46 minutes is not observed in the COVA model (Figure 11(i) and 12(i)).

Figure 10(e) shows the result of ICOVA modelling, where noise signals have been isolated and modelled individually. Traffic noise events and the pause in well site noise reflect the times that they occur in the recorded noise. Similar to Figure 9, the individual modelled noise signals are shown in Figure 13. The 60 Hz band-passed trace is of constant amplitude in time yet it is of lower magnitude in comparison to the recorded 60 Hz noise. In the frequency domain, the modelling has resulted in a smearing of the 60 Hz noise across nearby frequencies. The smearing of frequencies is observed on all noise signal models, particularly on the well site noise which experiences strong frequency banding. The car signal model provides a good approximation although the duration of the event is of slightly different shape and lasts longer than in the identified traffic noise (Figure 9(b)).

To provide a quantitative measure of how accurately the ICOVA models represent the original noise model realisations, MWW tests were performed to give a probability of the likelihood that the two datasets originate from the same distribution. For each noise signal model the MWW tests were performed between recorded noise and the modelled noise, over the modelling realisation parameters, with the results shown in Table 2. All the noise models have over 65% of MWW results with a greater than 50% probability of arising from the same distribution. The well site noise has the greatest likelihood of models and patches arising from the

same distribution with only 4% of MWW results having a probability of less than 25%. All models have less than 12% of realisations with a low chance ($P < 25\%$) of arising from the same distribution therefore the models provide a reasonable representation of the statistics of the recorded noise signals.

Figure 10(f) illustrates the result of the ICOVA-LPF model, where the LPF method has been used to gain a more realistic representation of the traffic event. The stationary background noise and pseudo-non-stationary well noise were modelling using the ICOVA method while the traffic noise, shown in Figure 14, is modelled using the ICOVA-LPF method. Modelling traffic events using an ICOVA-LPF provides a closer representation of the recorded noise signal and results in less frequency smearing, as is observable at 60Hz on Figure 14. However, the full hour of recorded noise for modelling has seven different traffic events and to fully represent the variability of traffic noise then each event must be modelled individually.

Figure 15 shows the skewness and excess kurtosis calculated across the realisations for each spatio-temporal patch position. As seen in the initial Gaussianity analysis, kurtosis is the dominant property for identifying non-Gaussianity. The well site noise realisations are the nearest to a multivariate Gaussian distribution and this may explain their higher MWW results while the traffic noise is highly non-Gaussian. To provide a constraint on the minimum number of patches required to get a stable estimation of the sample mean, Figure 16 shows the convergence of the sample mean for increasing number of patches for each noise type. It can be seen that for all noise types more than 200 realisations are required to get a near-convergence of the sample mean. Beyond 200, the change in mean through the addition of patches still fluctuates however they are of a significantly lower amplitude and so are considered negligible.

# 6 Discussion

Based on the noise analysis, it is evident that the spatial and temporal trends observed in the passive seismic data contradict the assumption of stationary, white and Gaussian noise. For example, Figure 4 shows considerable changes in the variance throughout the data. The figure also shows variance of the sample mean which we believe could come from one of two sources. Firstly, the variation maybe an artefact of long-period drift of the sensor system. The second possibility is that these variations are the imprint of changes in the variability of trace amplitudes on the measurement of the sample means.

With respect to the Gaussianity of the full noise field, the method of statistical moments did not detect any spatio-temporal trends in the recorded noise field. The excess kurtosis results displayed a significantly higher variation than the skewness results implying that the fourth mathematical moment is likely to be the most

effective property for identifying non-Gaussianity of the noise distribution. While both the bicoherence and tricoherence analyses highlight the same spatial and temporal zones as being non-Gaussian (i.e. around the well site and the roadside stations), the amplification of the non-Gaussianity of these aspects observed on the tricoherence analysis complements the observation that kurtosis is the dominant non-Gaussian property of the noise. Based on the study by Groos and Ritter [2009], the negative excess kurtosis observed is likely to be due to dominating periodic signals from anthropogenic seismic sources such as generators.

The ICOVA modelling method assumes that the noise field conforms to a multivariate Gaussian distribution as opposed to the single Gaussian distribution assumed in WGN modelling. In other words, under the WGN model the amplitude of noise behaves independently of space and time, whereas this is not the case for the COVA and ICOVA model. This allows each index point on a single recorded patch to have a separate mean and variance value (i.e. each index point can originate from a different Gaussian distribution). This condition requires that each index point across the patch realisations must arise from the same Gaussian distribution.

A significant benefit of modelling realistic noise, as opposed to directly incorporating recorded noise, is the ability to build a noise database of individual noise signals covariance matrix and mean vector. A database containing the necessary parameters for modelling a number of different noise signals provides the opportunity for creating 'tailor-made' noise models without any data collection or analysis required. This would provide flexibility around the occurrence of noise signals that is not possible when using recorded noise. The automation of noise signal identification and modelling which will significantly reduce manual labour time. From this study, there is the possibility for the incorporation of realistic noise into synthetic seismic datasets to test the robustness of detection and imaging algorithms against the different noise signals and magnitude. Furthermore, the identification of these noise signals and characteristics within the recorded data provides the possibility that the statistical properties of noise can be exploited for noise removal purposes.

# 7 Conclusions

This paper has introduced a novel method for improved realism of modelling noise observed in seismic data. The noise analysis determined that the noise field is not white or stationary and does not conform to a single Gaussian distribution, contrary to conventional assumptions in noise modelling techniques. We have shown that noise is made up of multiple signals that should be modelled separately to maintain their individual properties. We propose doing this using the isolated covariance modelling method, where the noise is assumed to arise from a multi-variate Gaussian distribution. Linear prediction filter modelling was

demonstrated as an alternative modelling technique when the assumptions for isolated covariance modelling are not met. We have developed a workflow to incorporate realistic noise models within synthetic seismic datasets. In the future this will provide a more robust opportunity to test and analyse how detection and imaging algorithms respond under realistic noise conditions. Furthermore, the developed workflow can be used to classify individual noise signals and their properties (for example, 9) which could possibly be used to guide noise removal techniques. This is becoming increasingly important given recent interest in stochastic interferometric methods for passive seismic data that are based on the assumption that noise (i.e., sources) have random distribution and amplitude characteristics (i.e., not coherent) [Schuster, 2009].

## Acknowledgements

The authors would like to thank Ray Chambers, Frans Kets and Lisa Roach for valuable discussions during this study. We would like to thank the Petroleum Technology Research Centre (PTRC) for access to Aquistore Data. Aquistore an independent research and monitoring project managed by the PTRC which intends to demonstrate that storing liquid carbon dioxide (CO2) deep underground (in a brine and sandstone water formation), is a safe, workable solution to reduce greenhouse gases (GHGs). C. Birnie is funded by the NERC Open CASE studentship NE/L009226/1 and Pinnacle-Halliburton. D. Angus acknowledges the Research Council UK (EP/K035878/1; EP/K021869/1; NE/L000423/1) for financial support.

## References

M. Asten and J. Henstridge. Array estimators and the use of microseisms for reconnaissance of sedimentary basins. *Geophysics*, 49(11):1828–1837, 1984.

M. W. Asten. Geological control on the three-component spectra of rayleigh-wave microseisms. *Bulletin of the Seismological Society of America*, 68(6):1623–1636, 1978.

C. Barajas-Olalde and A. Jeffreys. Seismic wind noise experiments using a portable wind tunnel. In *76th EAGE Conference and Exhibition 2014*, 2014.

T. Bardainne, E. Gaucher, F. Cerda, D. Drapeau, et al. Comparison of picking-based and waveform-based location methods of microseismic events: Application to a fracturing job. In *2009 SEG Annual Meeting*. Society of Exploration Geophysicists, 2009.

H. Bartelt, A. W. Lohmann, and B. Wirnitzer. Phase and amplitude recovery from bispectra. *Applied Optics*, 23(18):3121–3129, 1984.

M. Bekara, L. Knockaert, A. Seghouane, and G. Fleury. Seismic signal denoising using model selection. In *Signal Processing and Information Technology, 2003. ISSPIT 2003. Proceedings of the 3rd IEEE International Symposium on*. IEEE, 2003.

N. Belayouni, A. Gesret, G. Daniel, and M. Noble. Microseismic event location using the first and reflected arrivals. *GEOPHYSICS*, 80:WC133–WC143, 2015.

G. Berkhout and G. Blacquière. From removing to using ghost reflections. In *SEG Technical Program Expanded Abstracts 2015*, 2015.

K. Berkner and R. O. Wells Jr. Wavelet transforms and denoising algorithms. In *Signals, Systems & Computers, 1998. Conference Record of the Thirty-Second Asilomar Conference on*, volume 2, pages 1639–1643. IEEE, 1998.

V. A. Bloomfield. *Using R for Numerical Analysis in Science and Engineering*. CRC Press, 2014.

S. Bonnefoy-Claudet, F. Cotton, and P.-Y. Bard. The nature of noise wavefield and its applications for site effects studies: a literature review. *Earth-Science Reviews*, 79(3):205–227, 2006.

P. Borgnat, P. Flandrin, P. Honeine, C. Richard, and J. Xiao. Testing stationarity with surrogates: A time-frequency approach. *Signal Processing, IEEE Transactions on*, 58(7):3459–3470, 2010.

K. Chambers, J. Kendall, S. Brandsberg-Dahl, J. Rueda, et al. Testing the ability of surface arrays to monitor microseismic activity. *Geophysical Prospecting*, 58(5):821–830, 2010.

V. Chandran, S. Elgar, and B. Vanhoff. Statistics of tricoherence. *Signal Processing, IEEE Transactions on*, 42(12):3430–3440, 1994.

W. Collis, P. White, and J. Hammond. Higher-order spectra: the bispectrum and trispectrum. *Mechanical systems and signal processing*, 12(3):375–394, 1998.

T. Dean, J. C. Dupuis, and R. Hassan. The coherency of ambient seismic noise recorded during land surveys and the resulting implications for the effectiveness of geophone arrays. *Geophysics*, 80(3):P1–P10, 2015.

D. Draganov, K. Wapenaar, and J. Thorbecke. Passive seismic imaging in the presence of white noise sources. *The Leading Edge*, 23:889892, 2004.

J. Drew, P. Primiero, K. Brook, D. Raymer, T. Probert, A. Kim, and D. Leslie. Microseismic monitoring field test using surface, shallow grid and downhole arrays. In *SEG Expanded Abstracts*, volume 31, 2012.

R. A. Fisher. Moments and product moments of sampling distributions. *Proceedings of the London Mathematical Society*, pages 199–238, 1930.

F. Forghani-Arani. *Analysis and suppression of passive noise in surface microseismic data*. PhD thesis, Colorado School of Mines, 2013.

F. Forghani-Arani, M. Batzle, J. Behura, M. Willis, S. S. Haines, and M. Davidson. Noise suppression in surface microseismic data. *The Leading Edge*, 31(1496–1501):1496–1501, 2012.

P. J. Green, E. J. Kelly, and M. Levin. A comparison of seismic array processing methods. *Geophysical Journal of the Royal Astronomical Society*, 11:6784, 1966.

S. Grion, R. Telling, and J. Barnes. Adaptive de-ghosting by kurtosis maximisation. In *77th EAGE Conference and Exhibition 2015*, 2015.

J. Groos and J. Ritter. Time domain classification and quantification of seismic noise in an urban environment. *Geophysical Journal International*, 179(2):1213–1231, 2009.

B. Gutenberg. Microseisms. *Advances in Geophysics*, 5:53–92, 1958.

A. Kahrizi, M. Emdadi, and H. Karslı. Efficiency of complex trace analysis to attenuate ground-roll noise from seismic data. *Journal of Applied Geophysics*, 106:50–59, 2014.

Y.-G. Li, K. Aki, D. Adams, A. Hasemi, and W. H. Lee. Seismic guided waves trapped in the fault zone of the landers, california, earthquake of 1992. *Journal of Geophysical Research: Solid Earth (1978–2012)*, 99 (B6):11705–11722, 1994.

E. Lunedei and D. Albarello. Horizontal-to-vertical spectral ratios from a full-wavefield model of ambient vibrations generated by a distribution of spatially correlated surface sources. *Geophysical Journal International*, 201(2):1140–1153, 2015.

D. L. Massart, B. Vandeginste, S. Deming, Y. Michotte, and L. Kaufman. Chemometrics: a textbook. 1988.

S. Maxwell. *Microseismic Imaging of Hydraulic Fracturing: Improved Engineering of Unconventional Shale Reservoirs*. Number 17. SEG Books, 2014.

E. Nørmark. Wind and rain induced noise on reflection seismic data. In *Near Surface 2011-the 17th European Meeting of Environmental and Engineering Geophysics*, 2011.

P. O'Brien. Aspects of seismic research in the oil industry. *Geoexploration*, 12(2):75–96, 1974.

R. Pearce and B. Barley. The effect of noise on seismograms. *Geophysical Journal International*, 48(3): 543–547, 1977.

L. A. Pflug. Principal domains of the trispectrum, signal bandwidth, and implications for deconvolution. *Geophysics*, 65(3):958–969, 2000.

R. D. Pierce. Application of the positive alpha-stable distribution. In *Higher-Order Statistics, 1997., Proceedings of the IEEE Signal Processing Workshop on*, pages 420–424. IEEE, 1997.

D. Price, D. Angus, K. Chambers, and G. Jones. Surface microseismic imaging in the presence of high-velocity lithological layers. *Geophysics*, 80:WC117–WC131, 2015.

M. B. Priestley. *Non-linear and non-stationary time series analysis*. Academic Press London, 1988.

N. Riahi and P. Gerstoft. The seismic traffic footprint: Tracking trains, aircraft, and cars seismically. *Geophysical Research Letters*, 42(8):2674–2681, 2015.

N. Riahi, A. Goertz, B. Birkelo, and E. H. Saenger. A statistical strategy for ambient seismic wavefield analysis: investigating correlations to a hydrocarbon reservoir. *Geophysical Journal International*, 192(1): 148–162, 2013.

L. A. Roach, D. J. White, and B. Roberts. Assessment of 4d seismic repeatability and co2 detection limits using a sparse permanent land array at the aquistore co2 storage site. *Geophysics*, 80(2), 2015.

L. L. Scharf. *Statistical signal processing*, volume 98. Addison-Wesley Reading, MA, 1991.

S. Schilke, T. Probert, I. Bradford, A. Özbek, and J. Robertsson. Use of surface seismic patches for hydraulic fracture monitoring. In *76th EAGE Conference and Exhibition 2014*, 2014.

G. T. Schuster. *Seismic interferometry*, volume 1. Cambridge University Press Cambridge, 2009.

J. Shao, J. Tang, C. Sun, D. Wu, and N. Li. Micro-seismic data denoising based on sparse representations over learned dictionaries. In *77th EAGE Conference and Exhibition 2015*, 2015.

B.-C. Sylvette, C. Cécile, B. Pierre-Yves, C. Fabrice, M. Peter, K. Jozef, and D. Fäh. H/v ratio: a tool for site effects evaluation. results from 1-d noise simulations. *Geophysical Journal International*, 167(2): 827–837, 2006.

C. Trifu, D. Angus, and V. Shumila. A fast evaluation of the seismic moment tensor for induced seismicity. *Bulletin of the Seismological Society of America*, 90(6):1521–1527, 2000.

J. Trojanowski and L. Eisner. Comparison of migration-based detection and location methods for microseismic events. In *77th EAGE Conference and Exhibition 2015*, 2015.

A. T. Walden and M. L. Williams. Deconvolution, bandwidth, and the trispectrum. *Journal of the American Statistical Association*, 88(424):1323–1329, 1993.

R. E. White. Signal and noise estimation from seismic reflection data using spectral coherence methods. *Proceedings of the IEEE*, 72(10):1340–1356, 1984.

T. Zhong, Y. Li, N. Wu, P. Nie, and B. Yang. A study on the stationarity and gaussianity of the background noise in land-seismic prospecting. *Geophysics*, 80(4):V67–V82, 2015.

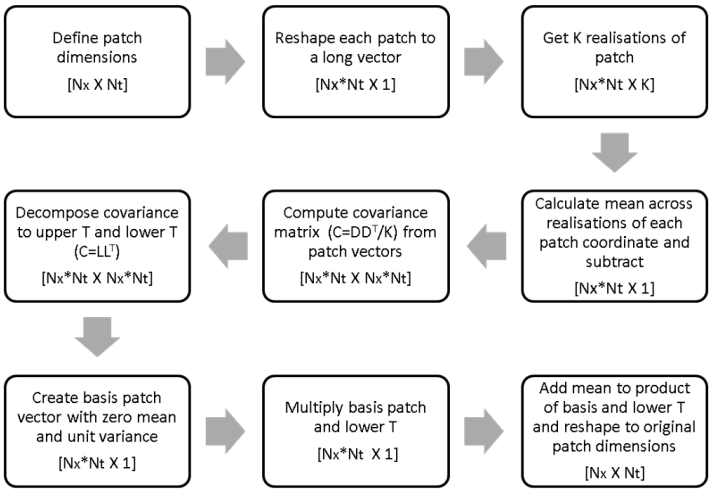


*Figure 1: Covariance-based modelling method work flow*

# Figures

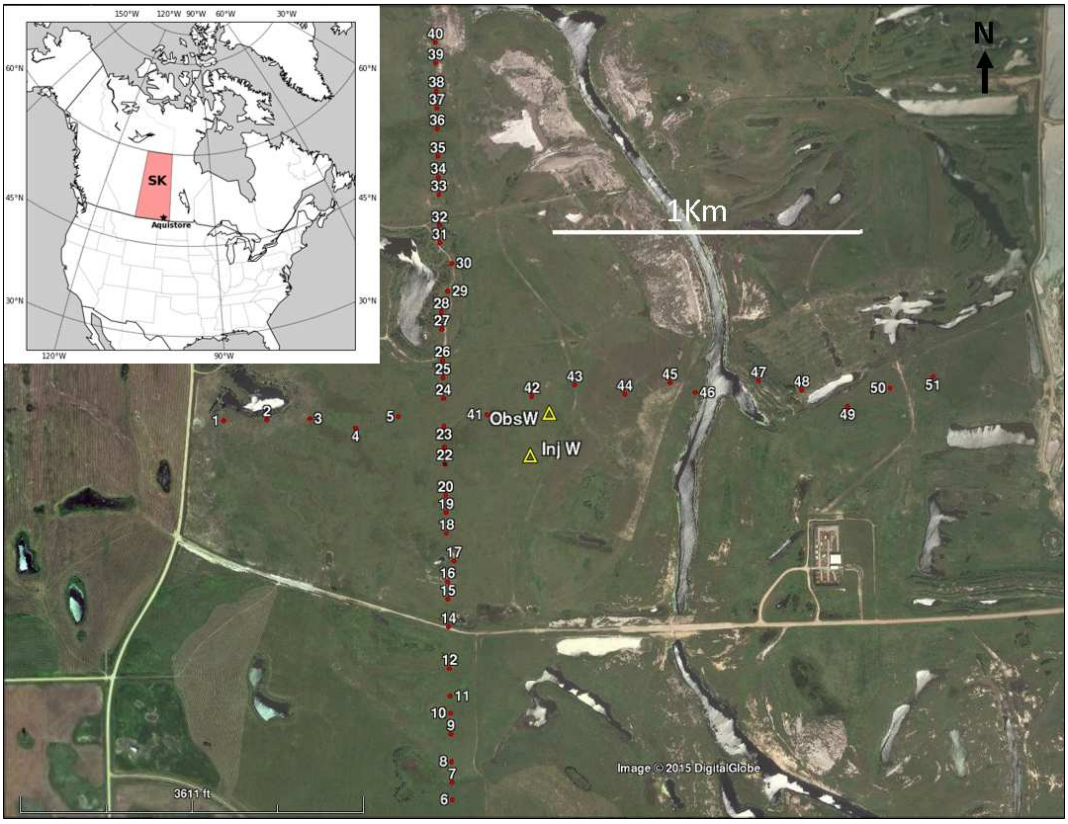


*Figure 2: Aquistore permanent seismic array survey geometry. Geophones are denoted by red dots alongside the station number, while the observation and injection wells are illustrated by yellow triangles.*

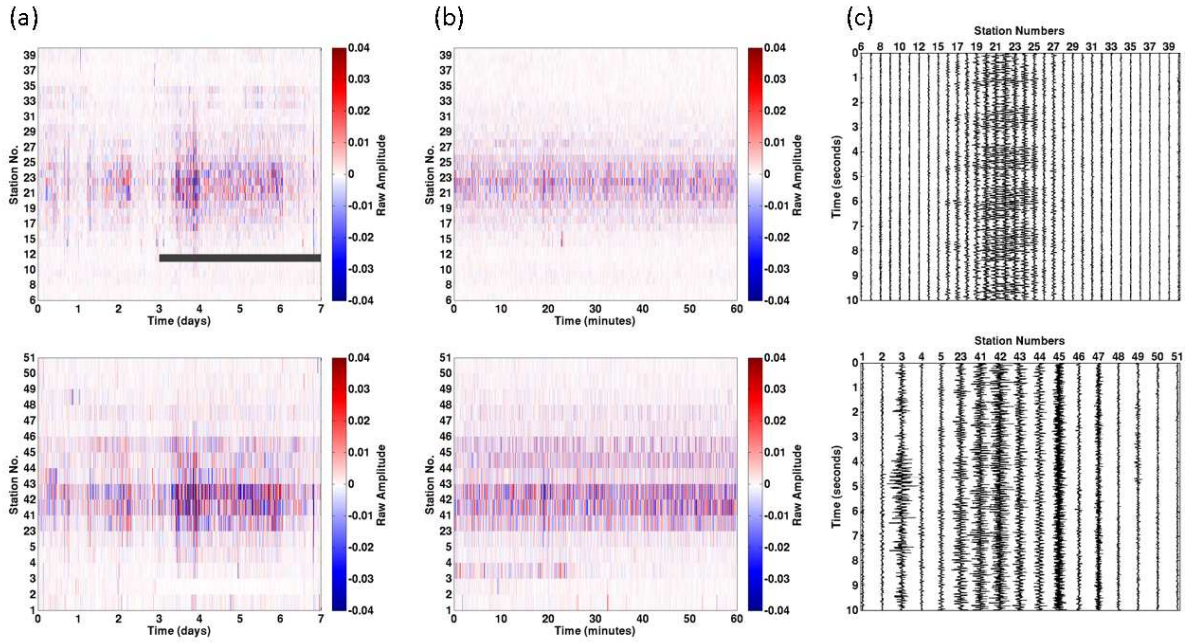


*Figure 3: Example of raw data used in the noise analysis for time periods of: (a) a week, (b) an hour and (c) ten seconds. Top row represents geophones on N-S profile and lower row represents geophones on E-W profile. Absent data is portrayed by a grey box.*

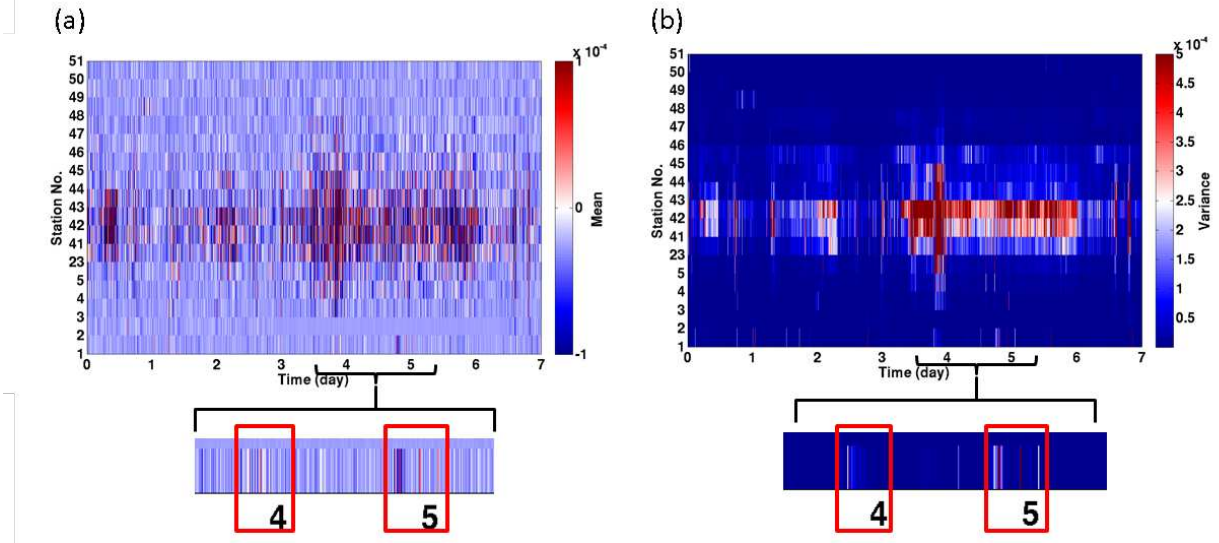


*Figure 4: (a) Mean and (b) variance results from sliding window analysis on a week of data from E-W geophone profile. Bottom inserts are zoomed in on roadside station (station 1) with daytime illustrated by the red boxes.*

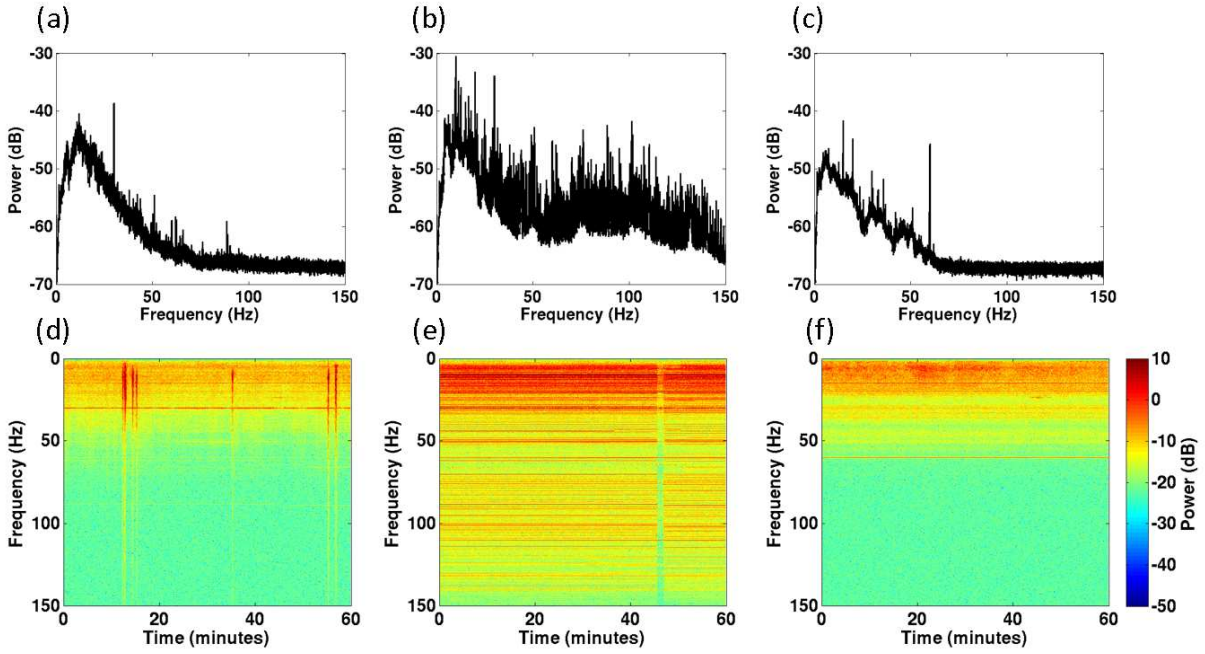


*Figure 5: Top row is the power spectral density from one hour of data at (a) station 1, (b) 42 and (c) 51. Lower row represents amplitude spectra calculated from a STFT for the same stations. Prior to converting to dB, each spectrum has been normalised to allow easy comparisons of the shapes of the spectra, this is required due to the uneven distribution of energy across the array as illustrated in Figure 6.*

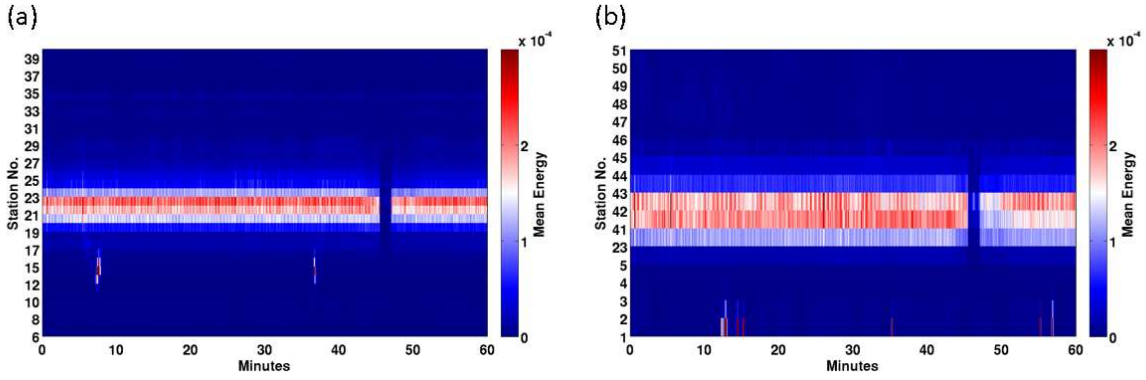


*Figure 6: Seismic energy (i.e. amplitude squared) across array for an hour of data from (a) N-S and (b) E-W profiles.*

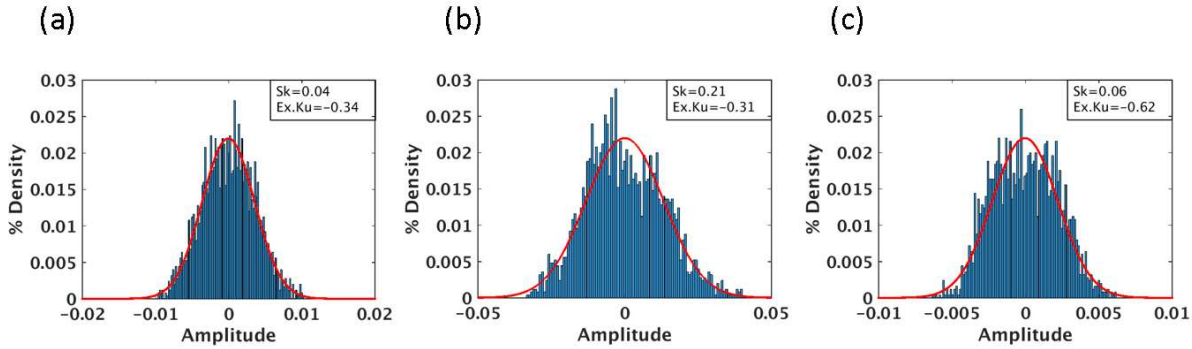


*Figure 7: Examples of three amplitude distributions and their skewness and excess kurtosis values for five seconds of data recorded from (a) station 45 at about 2 minutes, (b) station 42 at about 30 minutes, and, (c) station 12 at about 12 minutes. Overlain on each histogram is their respective Gaussian distribution.*

*Table 1: Calculated skewness and excess kurtosis values for an hour of recorded Aquistore data and Gaussian surrogate values.*

| | **Skewness** | | **Excess kurtosis** | |
|---|---|---|---|---|
| | *Aquistore* | *Gaussian* | *Aquistore* | *Gaussian* |
| **Mean** | -0.002 | 0.000 | -0.109 | -0.002 |
| **Maximum** | 49.98 | 0.27 | 2496.00 | 0.80 |
| **Minimum** | -19.58 | -0.26 | -1.65 | -0.41 |
| **% >0** | 49.71 | 50.00 | 26.45 | 47.15 |
| % <0 | 50.29 | 50.00 | 73.55 | 52.85 |
| **% >1** | 0.01 | 0.00 | 2.68 | 0.00 |
| **% <-1** | 0.04 | 0.00 | 2.71 | 0.00 |

# Tables

*Table 2: Percent of patch to model realisations likely to arise from the same distributions based on MWW tests*

| Noise Signal Models | Percent of realisations with $P > 75\%$ | Percent of realisations with $75\% > P < 50\%$ | Percent of realisations with $50\% > P < 25\%$ | Percent of realisations with $P < 25\%$ |
|---|---|---|---|---|
| Background | 34.5 | 30.6 | 23.3 | 11.7 |
| Well site | 41.9 | 34.2 | 19.2 | 4.4 |
| Traffic | 36.4 | 30.1 | 22.5 | 10.4 |

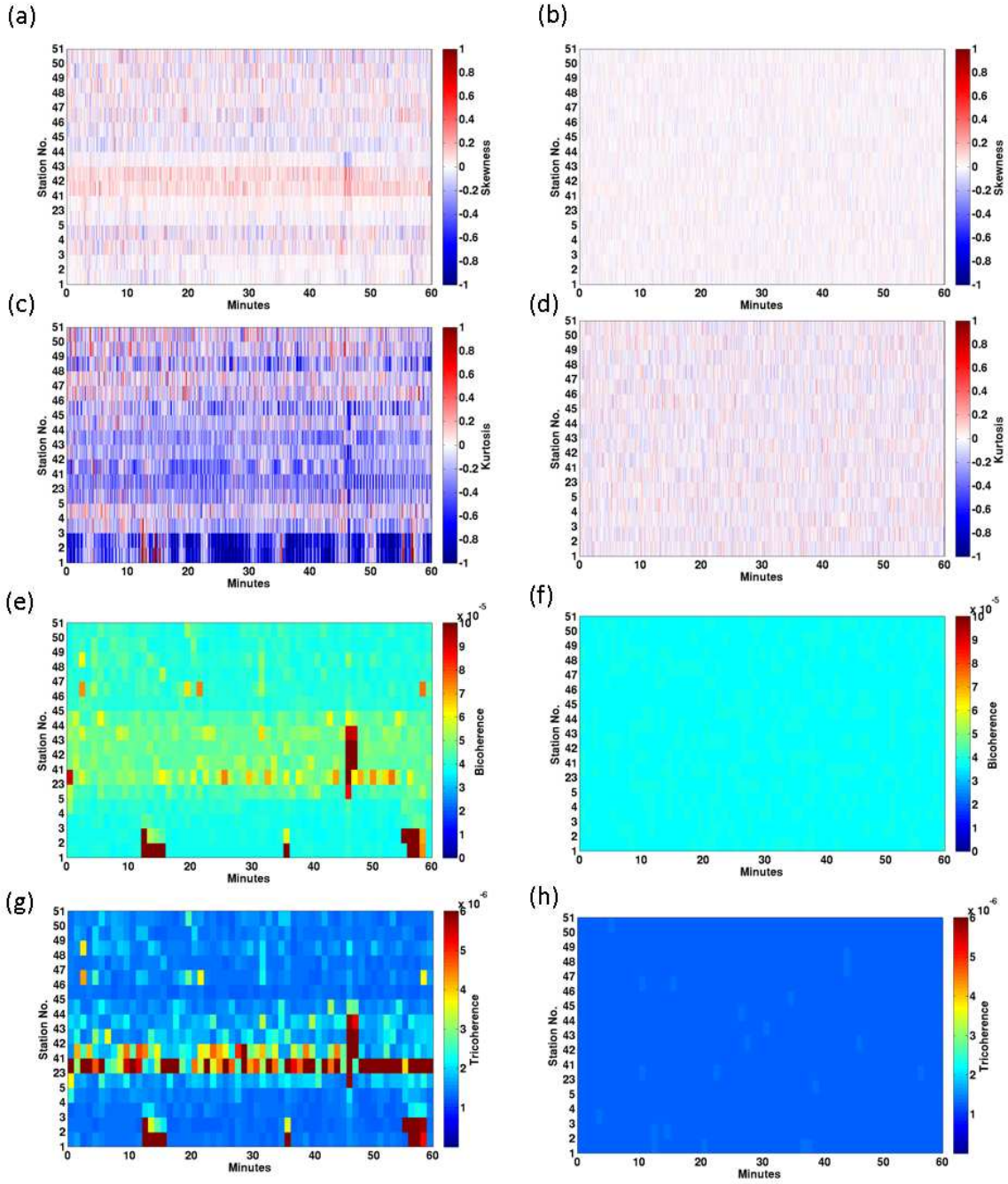


*Figure 8: (a),(b) Skewness for Aquistore and Gaussian surrogate noise respectively and (c),(d) kurtosis for Aquistore and Gaussian surrogate noise respectively, all calculated from sliding window analysis. (e),(f) Bicoherence for Aquistore and surrogate Gaussian noise respectively, and (g),(h) tricoherence for Aquistore and surrogate Gaussian noise respectively of an hour of data.*

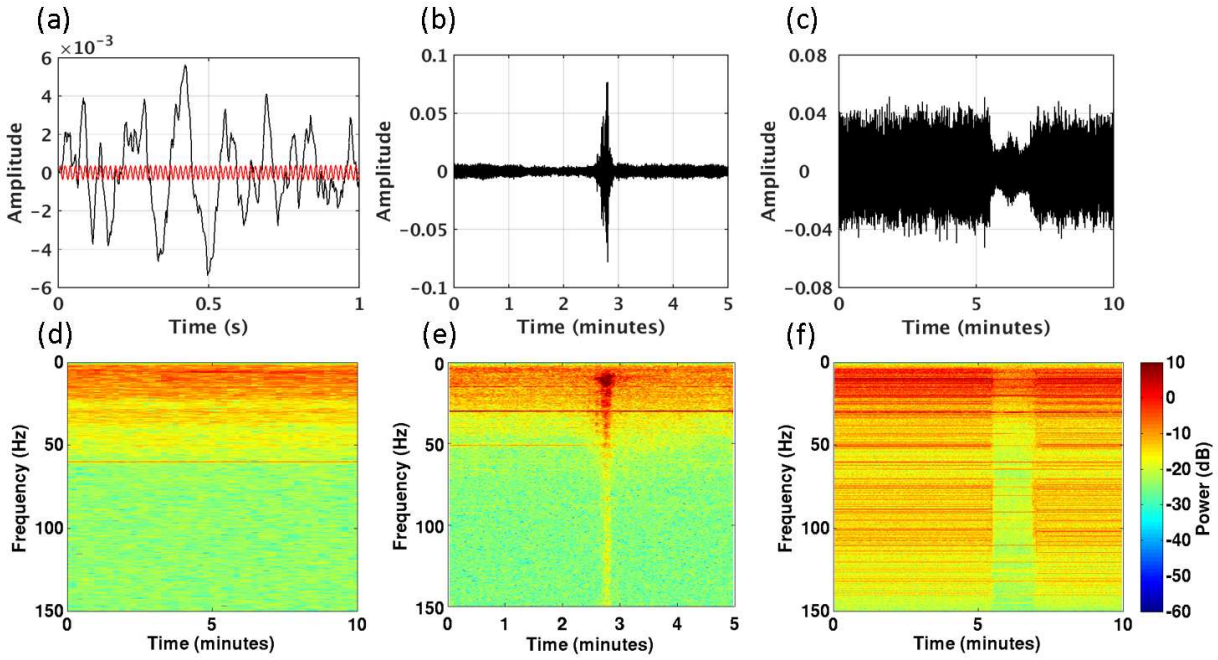


*Figure 9: Individual noise signals, (a),(d) stationary electrical interference observed at station 51 with red-trace denoting 60Hz band passed trace, (b),(e) non-stationary traffic signal observed at station one, and (c),(f) pseudo-non-stationary well site noise observed at station 42. Top row shows signals in time domain while portrays signals in the frequency domain.*

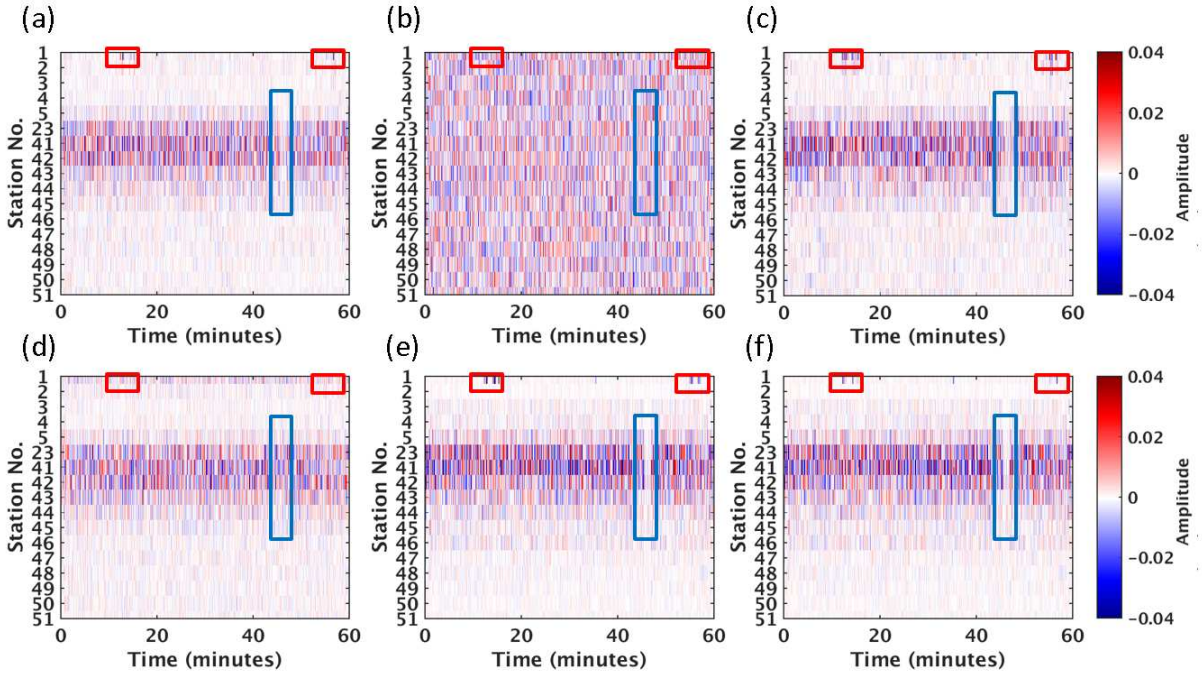


*Figure 10: (a) Hour of noise data from E-W profile used for modelling, where the red boxes indicate non-stationary traffic events at station 1 and the blue boxes indicate a pause in well site noise across the middle of the array. (b) WGN model, (c) CONV noise model, (d) single COVA noise field model and (e) sum of multiple COVA noise signal models.*

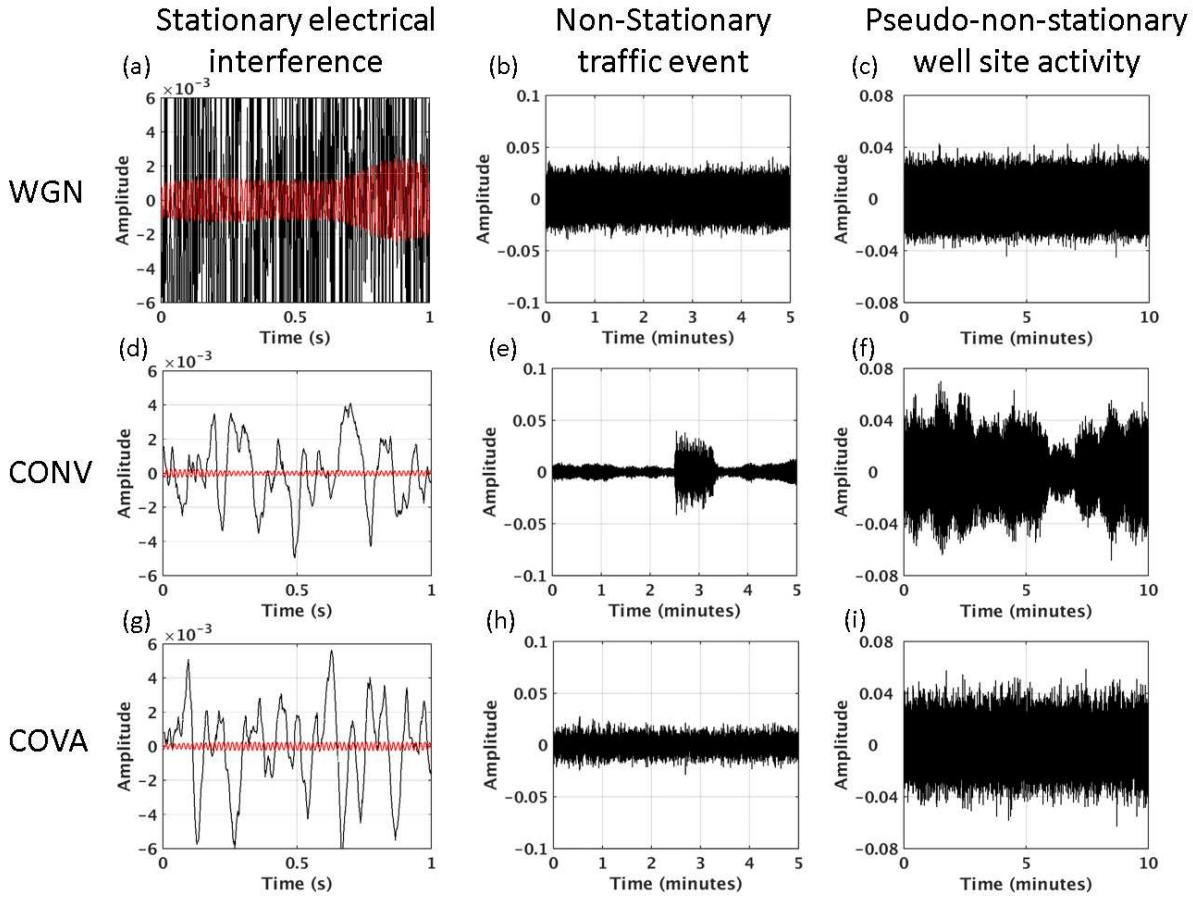


*Figure 11: Individual noise signals traces of stationary electrical interference (a,d,g), non-stationary traffic noise (b,e,h) and pseudo-non-stationary well site noise (c,f,i). The top row has traces from WGN model, the middle row has traces from the CONV model and the bottom row has traces from the COVA model. The red traces on the first column denote a 60Hz bandpassed trace.*

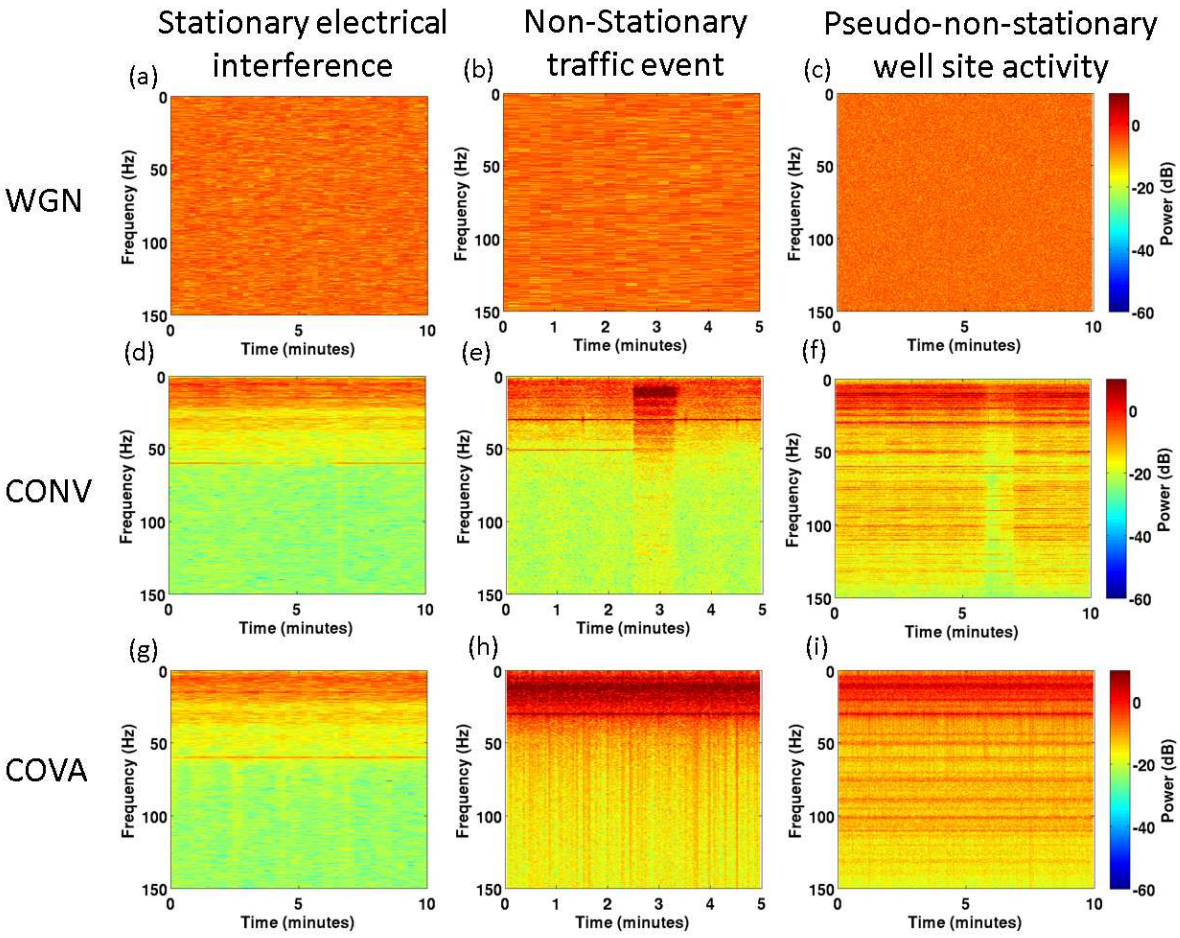


*Figure 12: Individual noise signals amplitude spectrum's of stationary electrical interference (a,d,g), non-stationary traffic noise (b,e,h) and pseudo-non-stationary well site noise (c,f,i). The top row has spectra from WGN model, the middle row has spectra from the CONV model and the bottom row has spectra from the COVA model.*

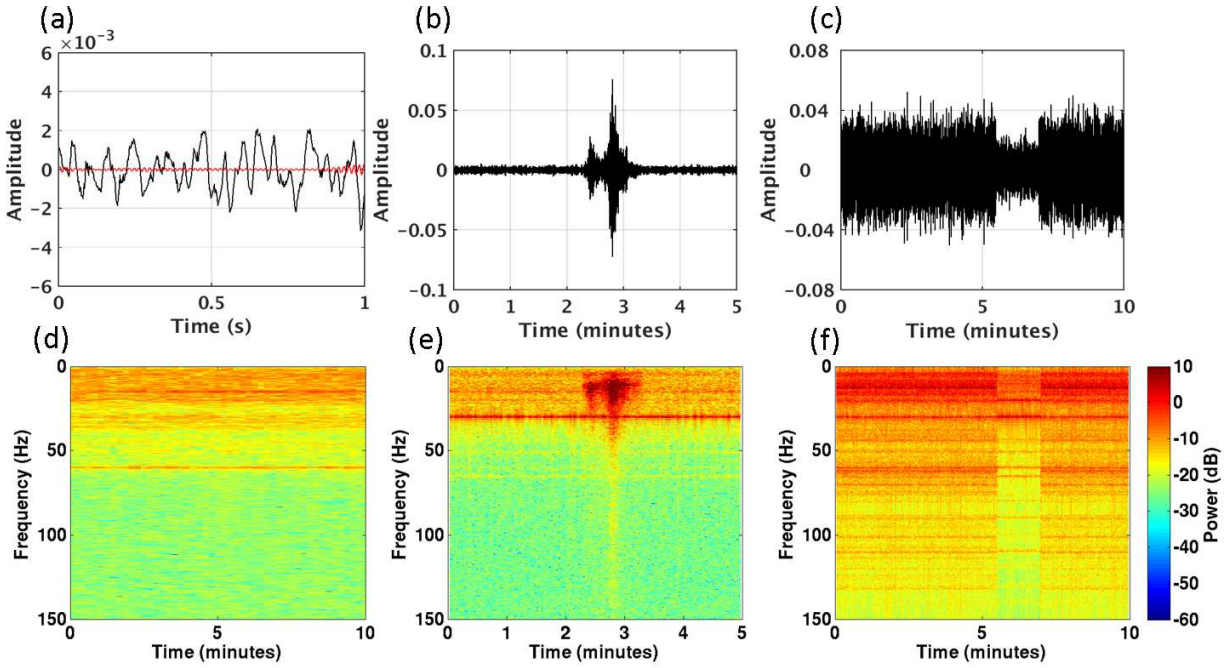


*Figure 13: Individual noise signals modelled by a sum of COVA models, (a),(d) stationary electrical interference observed at station 51 with red-trace denoting 60Hz band passed trace, (b),(e) non-stationary traffic signal observed at station 1, and (c),(f) pseudo-non-stationary well site noise observed at station 42. Top row shows signals in time domain while portrays signals in the frequency domain.*

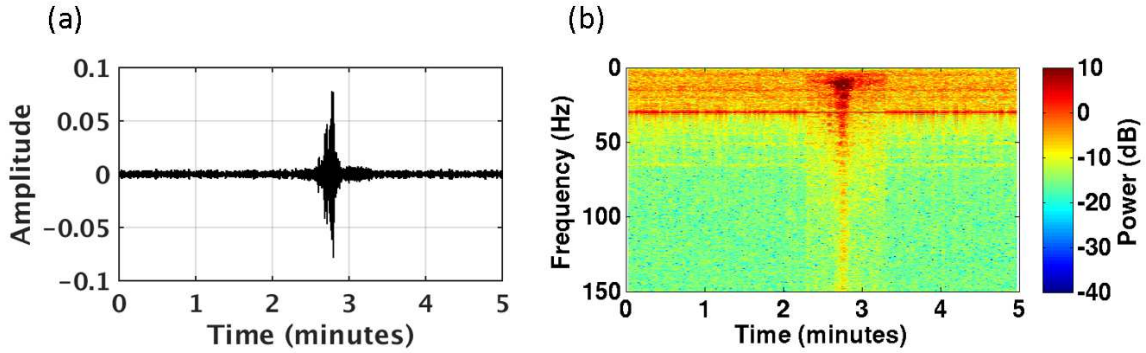


*Figure 14: A single traffic event, in time (a) and frequency (b), modelled using the autocorrelation method of AR modelling with background noise added from COVA noise model.*

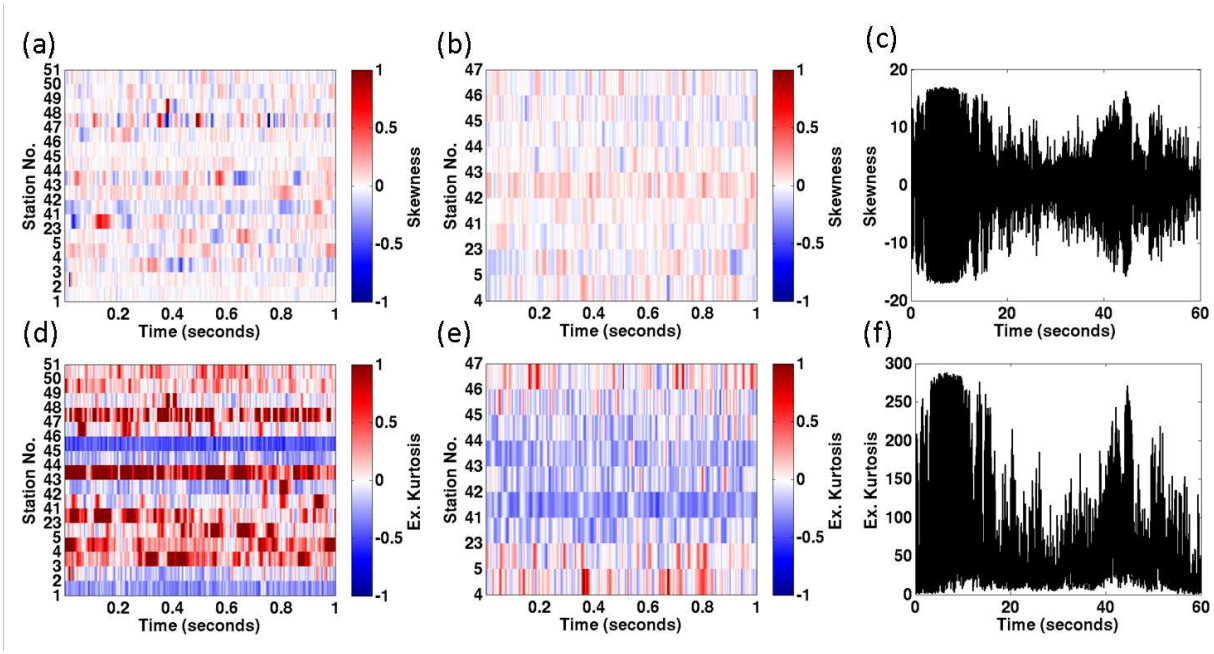


*Figure 15: Skewness (top row) and kurtosis (bottom row) of patch index points for (a) ICOVA stationary background noise model, (b) ICOVA pseudo-non-stationary well site noise model, and (c) ICOVA non-stationary traffic noise model.*

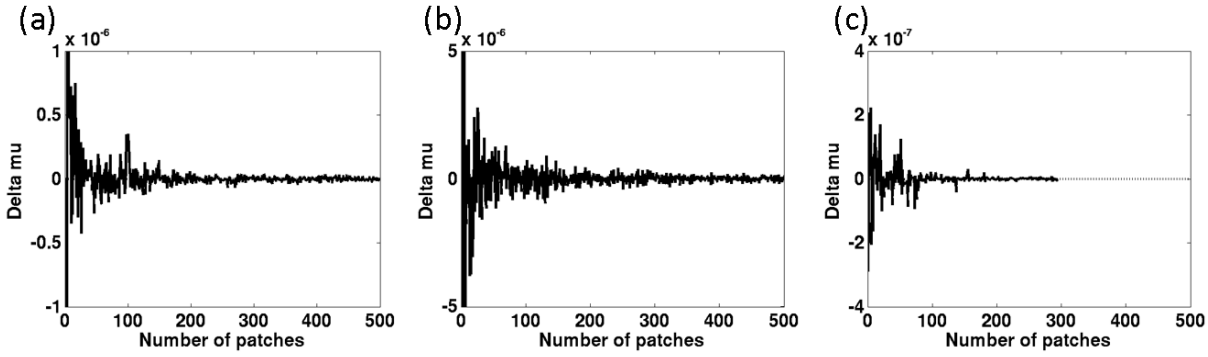


*Figure 16: Sample mean convergence over increasing number of noise patches for (a) ICOVA stationary background noise model, (b) ICOVA pseudo-non-stationary well site noise model, and (c) ICOVA non-stationary traffic noise model.*